

Old elliptical galaxies at $z \simeq 1.5$ and the Kormendy relation

I. Waddington^{1,2*}, R. A. Windhorst², S. H. Cohen², J. S. Dunlop³, J. A. Peacock³, R. Jimenez⁴, R. J. McLure⁵, A. J. Bunker^{6,7}, H. Spinrad⁷, A. Dey⁸ and D. Stern⁹

¹ *Department of Physics, University of Bristol, H. H. Wills Physics Laboratory, Tyndall Avenue, Bristol, BS8 1TL, UK*

² *Department of Physics & Astronomy, Arizona State University, PO Box 871504, Tempe, AZ 85287-1504, USA*

³ *Institute for Astronomy, University of Edinburgh, Royal Observatory, Blackford Hill, Edinburgh EH9 3HJ, UK*

⁴ *Department of Physics & Astronomy, Rutgers University, 136 Frelinghuysen Road, Piscataway, NJ 08854-8019, USA*

⁵ *Nuclear and Astrophysics Laboratory, University of Oxford, Keble Road, Oxford, OX1 3RH, UK*

⁶ *Institute of Astronomy, University of Cambridge, Madingley Road, Cambridge, CB3 0HA, UK*

⁷ *Astronomy Department, University of California at Berkeley, 601 Campbell Hall, Berkeley, CA 94720-3411, USA*

⁸ *KPNO/NOAO, 950 North Cherry Avenue, P. O. Box 26732, Tucson, AZ 85726, USA*

⁹ *Jet Propulsion Laboratory, California Institute of Technology, Mail Stop 169-327, Pasadena, CA 91109, USA*

Accepted 2002/07/19.

ABSTRACT

Deep spectroscopy of the two millijansky radio galaxies LBDS 53W069 and LBDS 53W091 has previously shown them to have old ($\gtrsim 3$ Gyr) stellar populations at $z \simeq 1.5$. Here we present the results of *Hubble Space Telescope* (*HST*) observations with the Wide Field and Planetary Camera 2 (WFPC2) in F814W and with the Near-Infrared Camera and Multi-Object Spectrograph (NICMOS) in F110W. We find that 53W069 has a de Vaucouleurs $r^{1/4}$ profile in both the F814W & F110W data with a mean effective radius of $0''.30 \pm 0''.06$ (2.7 ± 0.5 kpc). The restframe $U - B$ colour gradient is consistent with that of present-day ellipticals, requiring a stellar population of super-solar ($3Z_{\odot}$) metallicity that formed on a very short timescale at high redshift ($z > 5$). 53W091 has a regular $r^{1/4}$ profile in F110W with an effective radius of $0''.32 \pm 0''.08$ (2.9 ± 0.7 kpc). The F814W profile is more extended and is consistent with the presence of a blue exponential disk that contributes $20 \pm 10\%$ of the flux within r_e . We find a restframe $U - B$ colour gradient which is significantly larger than that observed in field ellipticals at $z \leq 1$, implying a stellar population of mixed metallicity ($1-3Z_{\odot}$) that formed in a high-redshift rapid burst.

We have compared these two LBDS radio galaxies with the Kormendy relations of ten 3CR radio galaxies at $z \simeq 0.8$ and a sample of cluster ellipticals at $z \sim 0.4$. The LBDS galaxies follow the Kormendy relation for the more radio-luminous 3CR galaxies, assuming passive evolution of their stellar populations, although they are smaller than the 3CR galaxies whose mean effective radius is 12 kpc. Their sizes and radio luminosities are consistent with scaling relations applied to the 3CR galaxies, in which both radio power and effective radius scale with galaxy mass. Compared with the sample of cluster ellipticals, 53W069 & 53W091 lie well within the scatter of the Kormendy relation. We conclude that the hosts of these millijansky radio sources at $z \simeq 1.5$ are passively-evolving elliptical galaxies that will evolve into ordinary L^* ellipticals by the present day.

Key words: galaxies: active — galaxies: elliptical and lenticular, cD — galaxies: evolution — galaxies: individual (LBDS 53W069, LBDS 53W091)

* Email: I.Waddington@bristol.ac.uk

1 INTRODUCTION

How did elliptical galaxies form and evolve? There are two mechanisms that have been proposed. First is the monolithic collapse model, in which elliptical galaxies form at high redshifts in an intense burst of star formation (Eggen, Lynden-Bell & Sandage 1962). Essentially all the final mass of the galaxy is already present within its potential well at the time of formation. The second mechanism is the merger model, in which ellipticals form at relatively lower redshifts from the merger of many smaller galaxies (e.g., Kauffmann & Charlot 1998). In this model, the mass of the galaxy increases with time as more and more smaller galaxies are cannibalized by the forming elliptical.

Recent observations suggest that both mechanisms may have a role to play. For example, Ellis et al. (1997) found that spheroidal galaxies in clusters at $z \simeq 0.5$ required a formation redshift (by which we mean the redshift at which the dominant stellar population formed) of $z_f \geq 3$. In contrast, Zepf (1997) found that the small number of very red galaxies in deep optical/infrared surveys suggested either that ellipticals form at moderate redshifts (and are enshrouded by dust), or that they assemble through the merging of smaller galaxies. Similarly Pascarelle et al. (1996) identified a group of Lyman- α emitters at $z = 2.39$ that they suggested may subsequently merge at a lower redshift into one or more luminous galaxies. Treu & Stiavelli (1999) concluded from their study of NICMOS parallel fields that a significant fraction (10–66%) of the elliptical galaxy population formed at $z_f \geq 3$, but the rest may have been formed (or at least assembled) at lower redshifts.

One important method of studying high-redshift ($z \gtrsim 1$) ellipticals is via radio selection. At low redshifts, luminous radio sources are almost exclusively hosted by giant elliptical galaxies containing old stellar populations (e.g., Kron, Koo & Windhorst 1985; Taylor et al. 1996; Nolan et al. 2001a). To the extent that radio galaxies at high redshifts are also hosted by giant ellipticals, they can be used to study the evolution of the elliptical galaxy population. Lilly & Longair (1984) obtained infrared K magnitudes for a subsample of the 3CR radio survey, from which they constructed a K -band Hubble diagram. They concluded from this K - z relation that luminous radio galaxies at $z \sim 1$ are giant ellipticals with passively-evolving stellar populations. Lilly et al. (1985) and Dunlop & Peacock (1990) found that the K - z relation for less-powerful radio galaxies led to a similar conclusion.

At redshifts $z \gtrsim 0.6$, Eales et al. (1997) found that the 6C radio galaxies, with radio luminosities a factor of ~ 5 lower than the 3CR, were also on average 0.6 mag fainter than 3CR in the K -band. Roche et al. (1998) investigated the K' -band morphologies of ten of these 6C sources at $z \sim 1.1$, showing that seven of them were normal ellipticals and the other three were ongoing or recent mergers. The radii of the 6C galaxies were significantly smaller than those of the 3CR sources at similar redshifts (Best et al. 1998; Zirm et al. 1999; McLure & Dunlop 2000), indicating that their fainter K magnitudes were due to their smaller size, not solely due to the difference in power of their AGN.

The Leiden-Berkeley Deep Survey (LBDS; Windhorst et al. 1984; Waddington et al. 2000), with a flux density limit of 1 mJy at 1.4 GHz, is sensitive to radio sources a

factor of ~ 200 fainter than the 6C survey, thus probing lower radio luminosities and higher redshifts. Windhorst, Keel & Pascarelle (1998) showed that the radio galaxy LBDS 53W002 has a weak AGN and a dominant $r^{1/4}$ profile with the colours of a $\sim 3 \times 10^8$ year young stellar population at $z = 2.39$, suggesting that these weak radio sources could have formed rather mature ellipticals at high redshifts. Two more of these sources have proved particularly useful for the study of galaxy evolution, due to the deep spectra that we obtained with the Keck telescope. LBDS 53W091 has a redshift of 1.552, and its restframe UV spectrum is best modeled by a stellar population ≥ 3.5 Gyr old (Dunlop et al. 1996; Spinrad et al. 1997). LBDS 53W069 is at $z = 1.432$ and has a best-fitting stellar population of age ≥ 4 Gyr (Dey 1997; Dunlop 1999b). Spinrad et al. (1997) investigated the age determination in detail and showed how the minimum age of the universe at $z \simeq 1.5$, as required by the age of 53W091, placed limits on the allowed values of the cosmological parameters (H_0 , Ω_M , Ω_Λ). Stockton et al. (1995) similarly showed that the age inferred from the Keck spectrum of the radio galaxy 3C65 (~ 4 Gyr at $z = 1.175$) required a formation redshift of $z_f \geq 5$.

Several authors have questioned the reliability of these age estimates, for example Bruzual & Magris (1999) and Yi et al. (2000) derive ages of 1.5–2 Gyr for 53W091. However, Dunlop (1999a) argued that such young ages are only deduced if the near-infrared photometry is included in the model fitting; if the fitting is confined to the spectroscopic data then a variety of stellar population synthesis codes consistently produce ages of ≥ 2.5 Gyr (see also Nolan et al. 2001b). We will not discuss this age controversy further here, but simply note that nothing in the current paper depends crucially on the precise ages of these sources.

In this paper we will investigate the morphologies of these two radio galaxies with the *Hubble Space Telescope's* (*HST*) Wide Field and Planetary Camera 2 (WFPC2) and Near-Infrared Camera and Multi-Object Spectrograph (NICMOS). At $z \simeq 1.5$, the 4000-Å break is straddled by the F814W and F110W filters, and thus the emission observed through these two filters is dominated by the young and old stellar populations respectively. In section 2, we describe the observations and discuss the processing steps that were applied to the data. In section 3, we investigate the surface brightness profiles and colour gradients of the two sources. The location of the galaxies on the Kormendy relation is the topic of section 4 and finally, in section 5, we comment on the apparent relations between radio luminosity, black-hole mass and effective radius of these sources. Our results are summarized in section 6.

We use AB magnitudes unless otherwise noted, and denote magnitudes in the three *HST* filters by I_{814} for F814W (WFPC2), J_{110} for F110W (NICMOS) and H_{160} for F160W (NICMOS). We assume a flat cosmology with $H_0 = 65 \text{ km s}^{-1} \text{ Mpc}^{-1}$, $\Omega_M = 0.3$, $\Omega_\Lambda = 0.7$.

2 OBSERVATIONS AND DATA REDUCTION

In 1997 August and 1997 October, we observed 53W069 and 53W091 with WFPC2 and NICMOS on the *HST*. 53W069 was observed for 2 orbits (a total integration of 5100 s) in F814W with WFPC2, and for 3 orbits (7680 s) in F110W

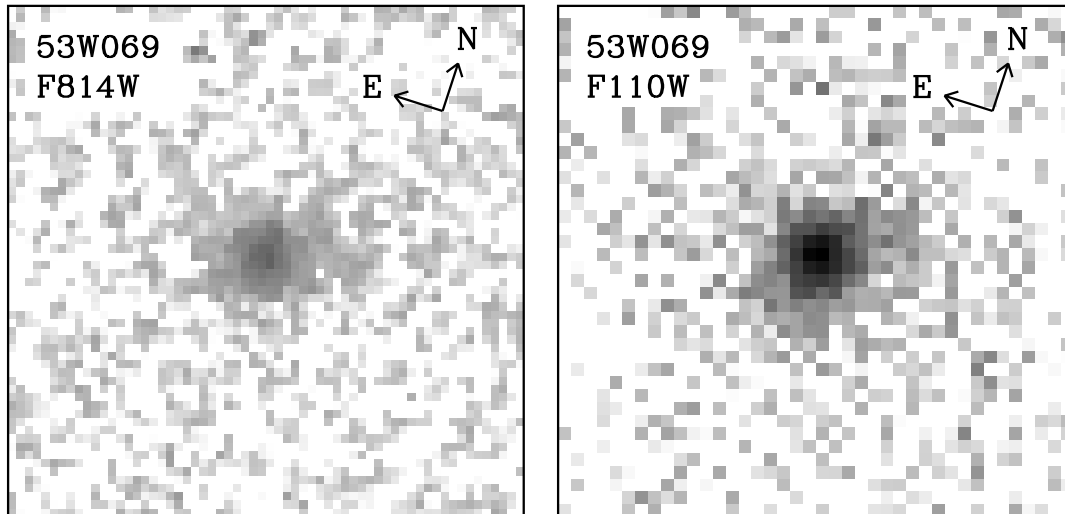


Figure 1. WFPC2 F814W and NICMOS F110W images of 53W069. The logarithmic grey-scale has been chosen so that both images have the same range in flux density (F_λ). Each image is 3×3 arcsec². The F814W image has been rotated in order to display it at the same orientation as the F110W image.

with NICMOS camera 2. 53W091 was observed for 2 orbits (5300 s) in F814W with WFPC2, and for 2 orbits (5120 s) in F110W with NICMOS camera 2. Each orbit devoted to WFPC2 imaging was split into two exposures, and consecutive orbits were offset by $0''.35$. In each orbit devoted to NICMOS imaging, five 512 s exposures were taken using a spiral dither pattern with $1''.91$ offsets. In 1998 August, we observed 53W091 and its companions for 10 orbits (25 600 s) in F160W with NICMOS camera 2. We independently analyse those data and describe the results in a complementary paper (Bunker et al. 2002).

The WFPC2 exposures were reduced using the standard pipeline processing (Voit 1997). For each target, the four dithered exposures were combined into a single image using the drizzling technique (Hook & Fruchter 1997; Fruchter et al. 1997). A pixel size of $0''.05$, one-half of the original pixel scale, was used, with a drop size of 0.6 (the parameter PIXFRACT). Offsets were calculated from the cross-correlation of ~ 10 bright sources in each exposure; no rotation was required. The drizzled images are shown in Figs 1 & 2.

We reduced the NICMOS images using a combination of processing techniques from STSDAS (Dickinson 1999) and our own methods. The raw images were partially processed with the standard pipeline task CALNICA, using the best reference files available from the STScI. We tried using the latest temperature-dependent darks in order to remove the shading, however we obtained better results with the standard dark reference files and used these instead. Non-linearities in the bias level of each image quadrant were removed with BIASEQ. Bias jumps were not corrected for in the data, as only one image was significantly affected and BIASEQ was not successful in removing the jumps. Cosmic rays were then removed by continued processing with CALNICA. The variable bias level from quadrant to quadrant, or “pedestal”, was corrected using the PEDSKY task, which also subtracted the sky

Table 1. Photometry

Source	Total AB magnitude		Colour*
	I_{814}	J_{110}	$I_{814} - J_{110}$
53W069	24.19 ± 0.03	22.45 ± 0.02	1.72 ± 0.05
53W091	24.14 ± 0.03	22.56 ± 0.03	1.57 ± 0.05

*The colours are defined in a circular aperture of $2''$ diameter.

background from the images. Then the data were flattened using CALNICA.

We applied a further correction to the data, adapted from standard ground-based infrared imaging methods. Since the NICMOS camera consists of four physically separate sub-arrays, we divided each partially-reduced image into its four separate quadrants. For each target, all the exposures of each quadrant were stacked and a median image calculated. Given that the exposures were dithered, this produced a map of the residual instrumental features (devoid of any astronomical objects) that were not removed by the flat-field reference file. These “super-sky” images for each quadrant were scaled to the mean of all four quadrants in order to preserve the quadrant-to-quadrant photometric accuracy. We then tried correcting each exposure by either (i) dividing by this super-sky after scaling it to have a mean of unity, or (ii) subtracting the super-sky from each exposure. For each object, we chose the method that produced the best image (i.e. the lowest rms noise). For the F110W images of both targets, *subtracting* the super-sky was most successful, suggesting that the instrumental features left after CALNICA processing were most likely due to incomplete dark subtraction. In particular, this removed the residual amplifier glow from the corners, while making a negligible difference to the center of the image, where the target was located (thus photometric accuracy had not been compromised by residual dark current beneath the target). Finally,

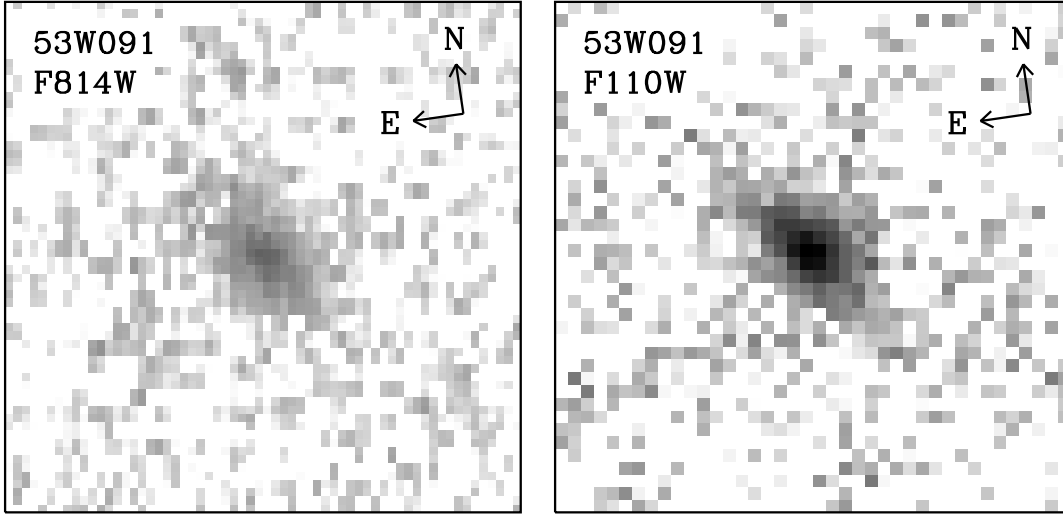


Figure 2. WFPC2 F814W and NICMOS F110W images of 53W091. The logarithmic grey-scale has been chosen so that both images have the same range in flux density (F_λ). Each image is 3×3 arcsec 2 . The F814W image has been rotated in order to display it at the same orientation as the F110W image, resulting in the apparent blurring of the drizzled data.

all the exposures were combined, on a quadrant by quadrant basis, to produce a mosaic for each object (Figs 1 & 2). The data were calibrated using the most recent photometric calibration parameters from the STScI.

The image detection program SEXTRACTOR (Bertin & Arnouts 1996) was used to calculate both aperture and total (“mag-auto”) AB magnitudes for the two radio galaxies in each of the filters. The results are given in Table 1. Although the total magnitudes give the best measurement of the flux detected in each individual image, the colours of the sources are properly defined in fixed apertures, thus we give the colours in Table 1 for $2''$ diameter circular apertures. We note that integration of the best-fitting model surface brightness profiles (see section 3.1 below) gives magnitudes consistent with these measurements.

3 MORPHOLOGIES

3.1 Surface brightness profiles

Surface brightness profiles were extracted for the two radio galaxies by fitting elliptical isophotes to the sky-subtracted images (Figs 3 & 4) with IRAF’s ELLIPSE routine. We fixed the centre of each isophote and allowed the position angle and axial ratio to vary freely. Model surface brightness profiles were extracted in the same way from two-dimensional exponential and de Vaucouleurs $r^{1/4}$ models convolved with a model point-spread function (PSF) from Tiny Tim (Krist & Hook 1999). The models were subsampled by a factor of 1, 2 or 5, convolved with a subsampled PSF and then resampled to the (drizzled) WFPC2 and NICMOS pixel size, before being extracted to a one-dimensional profile. The models were fitted to the data for $r > 1$ pixel, corresponding to $0''.05$ for WFPC2 (drizzled) and $0''.075$ for NICMOS – at smaller radii, the fit was dependent on the degree of subsampling of the PSF.

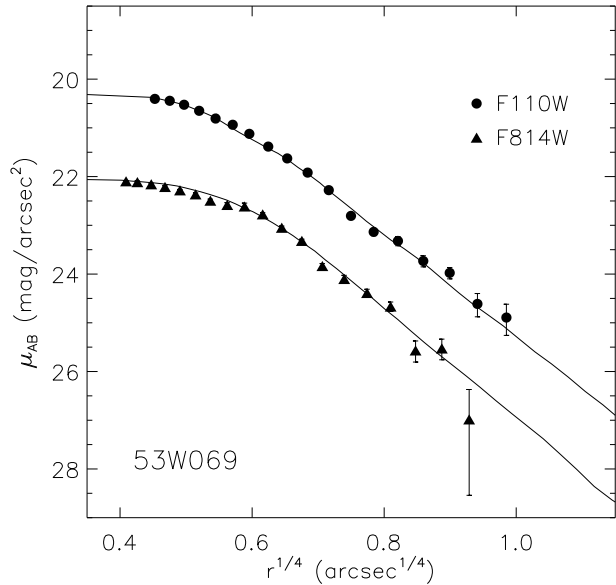


Figure 3. Surface brightness profiles along the major axis (points) and best-fitting models (lines) for 53W069. Both profiles follow a de Vaucouleurs $r^{1/4}$ law, with effective radii of $r_e = 0''.33$ in F110W and $r_e = 0''.28$ in F814W.

The best-fitting models for 53W069 are de Vaucouleurs $r^{1/4}$ profiles in both the F814W & F110W filters (Fig. 3). In F814W we find an effective radius of $r_e = 0''.28 \pm 0''.08$, and in F110W the profile is very similar with $r_e = 0''.33 \pm 0''.09$. The reduced chi-square for these models is $\chi_r^2 \simeq 2$, compared with a value of $\chi_r^2 \simeq 10$ for the best-fitting exponential models. The weighted mean of the F814W & F110W effective radii is $\bar{r}_e = 0''.30 \pm 0''.06$ or 2.7 ± 0.5 kpc. Morphologically, 53W069 is thus a relaxed elliptical galaxy, fully

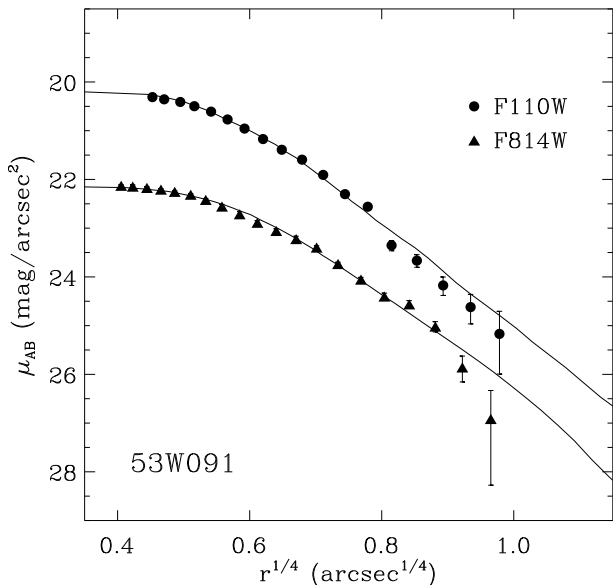


Figure 4. Surface brightness profiles along the major axis (points) and best-fitting models (lines) for 53W091. The F110W profile follows a de Vaucouleurs $r^{1/4}$ law, with effective radius of $r_e = 0''.32$. The F814W profile is the sum of an $r^{1/4}$ profile with effective radius $r_e = 0''.32$ plus an exponential with scale-length $r_0 = 0''.5$ contributing 20% of the flux within r_e .

consistent with its spectroscopic identification as an old, passively-evolving elliptical.

For 53W091, the best-fitting model in F110W is a de Vaucouleurs $r^{1/4}$ profile with $r_e = 0''.32 \pm 0''.08$ (Fig. 4). This model has a reduced chi-square value of $\chi_r^2 = 1.8$ compared with a value of $\chi_r^2 = 7.3$ for the best exponential model. In Bunker et al. (2002) we show that the F160W profile similarly follows a de Vaucouleurs law with $r_e = 0''.32 \pm 0''.03$. For the F814W profile, the best-fitting single component model is an $r^{1/4}$ profile with $r_e = 0''.6 \pm 0''.2$, for which $\chi_r^2 = 3.3$ (compared with $\chi_r^2 = 18$ for the best exponential model). Given the large difference between the effective radius of this best-fitting model and that of the F110W & F160W models, we also fitted the F814W profile with a two-component model. We used the best-fitting F110W/F160W de Vaucouleurs model with $r_e = 0''.32$ and added an exponential disk, varying both the scale-length of the exponential and the relative flux of the two components. The best-fitting composite model (with $\chi_r^2 = 2.6$) has a disk with scale-length $r_0 = 0''.5 \pm 0''.2$ (4 ± 2 kpc), that contributes $20 \pm 10\%$ of the flux within the half-light radius (Fig. 4). At $z = 1.552$, the F814W filter measures the galaxy’s restframe emission below the 4000-Å break, and is thus sensitive to bluer stars than F110W. Such a population will make an even less significant contribution to the flux at longer wavelengths, thus it is quite consistent that we do not see a disk component in the F110W data.

3.2 Colour gradients

The stellar population of an elliptical galaxy is not uniform, but varies with radius. This is seen as a gradient in the

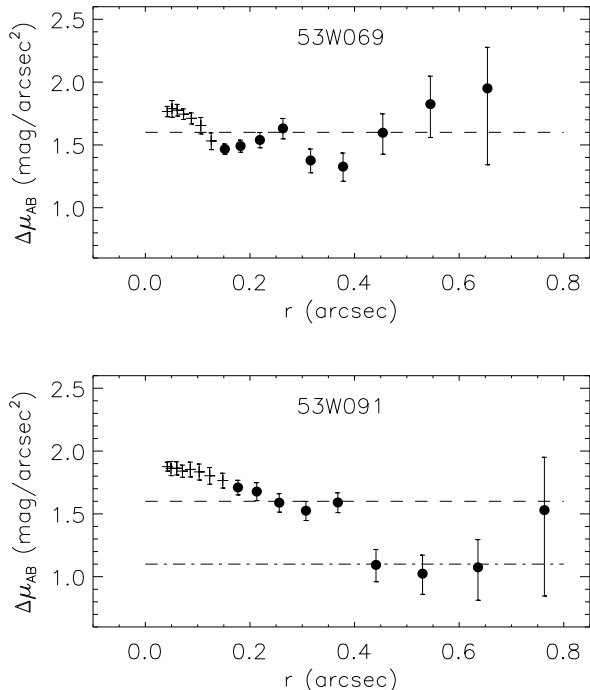


Figure 5. $I_{814} - J_{110}$ colour gradients for 53W069 & 53W091. Crosses denote data within the central two pixels for which pixelation effects and differences in the WFPC2 and NICMOS PSFs contribute as much as 0.1–0.3 mag to the colour gradient. The horizontal lines are the colours predicted by a high-redshift burst of star formation, for two different metallicities: solar (dot-dash line) and $3Z_{\odot}$ (dashed line).

colours of the galaxy, which become bluer with increasing radius (Franx et al. 1989; Peletier et al. 1990; Tamura et al. 2000). If 53W069 and 53W091 are the passively-evolving precursors to present-day ellipticals, we should expect to see such characteristic colour gradients. Peletier et al. (1990) show that the $U - B$ colour gradient of nearby ellipticals is -0.1 mag arcsec $^{-2}$ per dex in radius. The I_{814} and J_{110} bands of our radio galaxies at $z \simeq 1.5$ approximately correspond to rest-frame U and B , thus we should expect to see a gradient of the same order as Peletier et al. (1990).

In Fig. 5, we plot the colours of the two radio galaxies as a function of radius. Small differences between the (drizzled) WFPC2 and NICMOS PSFs dominate the colour gradients within the central 1–2 pixels. Specifically, the radii containing (50%, 90%) of the encircled energy are ($0''.08$, $0''.37$) and ($0''.08$, $0''.48$) for the WFPC2 F814W and NICMOS F110W PSF models respectively. Examination of our PSF-convolved galaxy models suggests that these differences result in artificially redder colours within the central pixels, contributing as much as 0.1–0.3 mag to the colour gradient at $r < 0''.15$ (crosses in Fig. 5). At larger radii this effect is less than 0.1 mag, so we restrict our discussion to $r > 0''.15$. Given the limited quality of the data and the absence of PSF stars in the NICMOS images, we decided there was little to be gained from attempting detailed PSF matching to better than 10%.

It can be seen in Fig. 5 that the errors in the $I_{814} - J_{110}$ colours of 53W069 are too large to measure a colour

change of -0.1 mag arcsec $^{-2}$ across the extent of the galaxy (less than 1 dex in radius). Thus the colours of 53W069 do not preclude a gradient comparable to that of present-day ellipticals, but they are also consistent with there being no colour gradient. Windhorst et al. (1994, 1998) similarly found little or no colour gradients in several other LBDS radio galaxies and field galaxies at $0.3 < z < 2.4$ observed with *HST*. In particular, any colour gradient in the elliptical radio galaxy 53W002 at $z = 2.39$ must be smaller than -0.3 mag across the $1''$ (9 kpc) image (Windhorst et al. 1998). The (restframe) $U - B$ gradients of early-type cluster and field galaxies at $z \simeq 0.4-1$ have been found to typically span -0.2 to 0.1 mag per dex in radius (Saglia et al. 2000; Hinkley & Im 2001), again consistent with 53W069.

In contrast, there is a significant gradient in the $I_{814} - J_{110}$ colour of 53W091. This gradient is in the same sense as that seen in nearby ellipticals (i.e., the galaxy is redder in the center and becomes more blue at larger radii), but it is much greater in magnitude. The best fit to the colours gives a gradient of -1.0 ± 0.2 mag arcsec $^{-2}$ per dex in radius. This clearly indicates the presence of an extended blue component in the galaxy’s morphology, and is consistent with the results of our model fitting above. There appears to be a “jump” in the colour gradient at $r \simeq 0''.4$ (see also the F110W profile), but this is not significant given the errors, and the data are consistent with a constant gradient out to $r \simeq 0''.6$. We note that the position angle (PA) of the major axis of the optical/infrared emission (~ 45 degrees) is perpendicular to the PA of the radio lobes (131 degrees; Spinrad et al. 1997), so it is unlikely that this extended blue emission is due to the radio–optical alignment effect. We emphasize that the difference in WFPC2 and NICMOS PSFs is unlikely to have produced this gradient because: (i) it is not seen in the data for 53W069; and (ii) the profile fitting above *includes* a convolution with the PSFs, and clearly shows that the galaxy is more extended (i.e. has a larger scale-length) in the F814W data than in the F110W data.

We compared the observed colour gradients of 53W069 and 53W091 with the predictions of single collapse multi-zone models of elliptical galaxies (Menanteau, Jimenez & Matteucci 2001b). We used an IMF with lower and upper cutoffs of $0.1 M_{\odot}$ and $120 M_{\odot}$ respectively, and a range of formation redshifts. None of the models could reproduce the observed gradients, demonstrating that the very red cores found in these two galaxies are inconsistent with an extended period of star formation in their centres. We then modified the models to force the star formation to stop after 0.05 Gyr. The resulting colours for two different metallicities, solar (Z_{\odot}) and $3Z_{\odot}$ are shown in Fig. 5. We find that the models fit the observed gradients if star formation took place on a short time scale in both galaxies and if they were formed at redshift $z > 5$. 53W069 is best fit by a population that has, on average, supersolar metallicity ($3Z_{\odot}$). 53W091 has a core that is metal-rich ($3Z_{\odot}$) and at larger radii ($r > 0''.4$) is better fit by a solar metallicity population.

These results are in excellent agreement with those of Nolan et al. (2002) who find that the *UV spectra* of these galaxies are similarly best-fit with populations of solar (53W091) and supersolar ($2Z_{\odot}$, 53W069) average metallicity. Studies of $z \simeq 0.4-1$ ellipticals similarly indicate that the colour gradients of early-type galaxies are due to metallicity gradients, falling from $\sim 2.5Z_{\odot}$ at the centre to solar in the

outer regions (Hinkley & Im 2001), although the observed gradients are not as steep as that in 53W091.

As discussed above, the best fit to the F814W profile of 53W091 is obtained by adding a disk-like exponential component to the best-fitting de Vaucouleurs profile measured in the F110W and F160W bands. Dunlop (1999a) showed that the difference between the restframe UV spectrum of 53W091 and that of 53W069 can be fitted by a blue stellar (F0V) spectrum, contributing 10–20% of the UV flux. Similarly, we have shown that $\sim 20\%$ of the restframe U -band flux within the half-light radius ($r_e = 0''.32$) could originate in a disk component. With a $1''$ slit and seeing of $0''.8-1''$, the spectroscopy of 53W091 was dominated by the flux within r_e , and we find consistency between the fraction of excess blue light in the spectroscopy and the disk component in the imaging. This extended blue component is also consistent with having lower metallicity than the core of the galaxy.

Combining these results leads us to conclude that 53W091 is either: (i) an elliptical galaxy with an old, metal-rich, passively-evolving stellar population (just like 53W069), surrounded by a faint disk of younger or lower-metallicity stars; or possibly (ii) an elliptical galaxy with an old, passively-evolving stellar population whose metallicity decreases with radius. We note that the age of the dominant red stellar population in 53W091 would have been somewhat underestimated due to the presence of a younger stellar component in the disk. Menanteau et al. (2001a) find that about half of field ellipticals at $z \sim 1$ must be undergoing recent episodes of star formation, due to their irregular internal colours and blue cores. The two radio galaxies 53W069 & 53W091, in contrast, belong to the other 50 per cent of field ellipticals that have evolved passively since very high redshifts.

4 THE KORMENDY RELATION

A key characteristic of dynamically relaxed elliptical galaxies is the existence of the Fundamental Plane (Djorgovski & Davis 1987; Dressler et al. 1987) – a scaling relation between the luminosity L , effective radius r_e and velocity dispersion σ of ellipticals: $L \propto r_e^a \sigma^b$. Given the difficulty of measuring velocity dispersions, particularly at high redshift, a more useful relation is the projection of the Fundamental Plane onto the effective radius–surface brightness (μ_e) plane, or the Kormendy relation (Kormendy 1977). Cluster ellipticals (Barger et al. 1998; Ziegler et al. 1999), field ellipticals (Schade et al. 1996) and radio galaxies (McLure & Dunlop 2000) have all been shown to follow the Kormendy relation out to $z \simeq 0.5-1.0$, assuming passive evolution of their stellar populations. Here we consider if our two high-redshift LBDS radio galaxies are consistent with these results. At $z \simeq 1.5$ the F110W filter approximately samples the restframe B -band. We thus compare the F110W data on 53W069 and 53W091 (Table 2) with two samples of elliptical galaxies observed with *HST* in restframe B .

4.1 Comparison with 3CR radio galaxies at $z \simeq 0.8$

In Fig. 6, we plot the surface brightness at the effective radius μ_e against the effective radius r_e for the two LBDS ra-

Table 2. Data for the F110W (restframe B -band) Kormendy relation. μ_e is the surface brightness at the effective radius (r_e), and $\langle\mu_e\rangle$ is the mean surface brightness within r_e .

Source	r_e (arcsec)	μ_e (mag arcsec $^{-2}$)	$\langle\mu_e\rangle$ (mag arcsec $^{-2}$)
53W069	0.33 ± 0.08	22.6 ± 0.1	21.7 ± 0.1
53W091	0.32 ± 0.08	22.4 ± 0.1	21.5 ± 0.1

dio galaxies and a sample of 3CR radio galaxies at $z \simeq 0.8$ (McLure & Dunlop 2000). The F110W and F814W filters both sample the rest-frame B -band at $z = 1.5$ and $z = 0.8$ respectively. We have thus corrected the J_{110} -band surface brightness of 53W069 & 53W091 to their equivalent I_{814} -band values at $z = 0.8$, minimizing any error introduced by the possible wavelength dependence of r_e . We made three corrections derived using the spectral synthesis models of both Fioc & Rocca-Volmerange (1997) and the 1996 revision of Bruzual & Charlot (1993). We used their elliptical and burst models respectively, and refer the reader to those papers for technical details such as IMFs. The F110W filter is significantly wider than F814W, thus requiring a K-correction of +0.6 mag to the F110W data. Second, passive evolution of +0.7 mag from 3 Gyr ($z = 1.5$) to 6 Gyr ($z = 0.8$) was derived using the burst/elliptical models. We set the age of the galaxies to be 3 Gyr at $z = 1.5$ and then evolved them in our chosen cosmology until $z = 0.8$. Third, the transformation from AB magnitudes to Vega magnitudes was -0.7 mag. All the sources, LBDS & 3CR, were corrected for the $(1+z)^4$ surface brightness dimming, placing them all at a common redshift of 0.8 (the 3CR sample has a narrow redshift range of ± 0.07 , and correspondingly small surface brightness corrections of $\lesssim 0.1$ mag). We tested the reliability of the corrections by using the two different sets of models (Bruzual/Charlot and Fioc/Rocca-Volmerange), and by varying the age of the LBDS galaxies at $z = 1.5$ by ± 1 Gyr, corresponding to the range of spectroscopic ages derived by ourselves (e.g., Dunlop et al. 1996) and others (e.g., Bruzual & Magris 1999). The combined uncertainty in K-corrections and evolution was ± 0.2 – 0.3 mag.

We have recalculated the normalization of the 3CR Kormendy relation for our cosmology, fixing the (cosmology-independent) slope at 3.2 (McLure & Dunlop 2000), and plot the fit in Fig. 6 (solid line). It is seen that 53W069 and 53W091 both lie on the 3CR Kormendy relation. The effective radii of the two LBDS galaxies ($r_e \simeq 3$ kpc) are much smaller than the mean effective radius of the 3CR sources ($\bar{r}_e = 12$ kpc), but they are comparable with the size of the smallest 3CR galaxy in this sample (3C340 with $r_e = 4.0$ kpc). McLure & Dunlop (2000) demonstrated that these 3CR galaxies follow a Kormendy relation that is indistinguishable from that of AGN hosts at $z \simeq 0.2$, assuming passive evolution of their stellar populations. Here we can extend that result to higher redshifts, concluding that there is no evidence for any significant dynamical evolution of the elliptical hosts of radio sources between $z \simeq 1.5$ and 0.2.

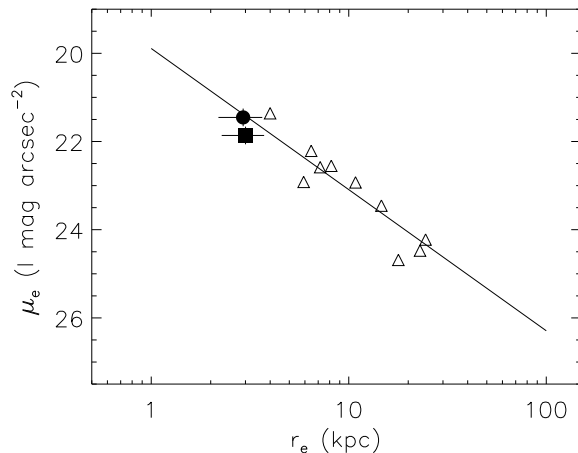


Figure 6. Effective surface brightnesses of 53W069 & 53W091 compared with the Kormendy relation of a sample of 3CR radio galaxies at $z \simeq 0.8$. 53W069 (square) & 53W091 (circle) have been corrected for: (i) surface brightness dimming, (ii) bandpass shift (observed F110W to F814W), and (iii) passive evolution, between $z \simeq 1.5$ and $z = 0.8$. The 3CR surface brightness data (triangles) have been corrected ($\lesssim 0.1$ mag) to a common redshift of 0.8. The solid line is the best-fitting Kormendy relation from McLure & Dunlop (2000), renormalized to a redshift of 0.8 and our cosmology.

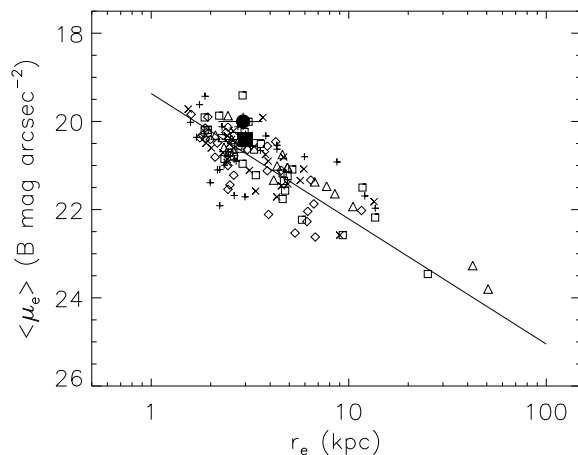


Figure 7. Mean surface brightnesses of 53W069 & 53W091 compared with the Kormendy relation of a sample of cluster ellipticals at $z \sim 0.4$. 53W069 (solid square) & 53W091 (solid circle) have been corrected for: (i) surface brightness dimming, (ii) bandpass shift (observed F110W to B), and (iii) passive evolution, between $z \simeq 1.5$ and $z = 0.0$. The cluster ellipticals have been taken from Ziegler et al. (1999), and have similarly been transformed to zero redshift. The clusters are: Abell 370 at $z = 0.375$ (triangles); Cl 1447+26 at $z = 0.389$ (diamonds); Cl 0939+47 at $z = 0.407$ (plus symbols); Cl 0303+17 at $z = 0.416$ (crosses); and Cl 0016+16 at $z = 0.55$ (squares). The solid line is a least squares bisector fit to the cluster data.

4.2 Comparison with cluster ellipticals at $z \simeq 0.4$

In Fig. 7, we compare the LBDS radio galaxies with cluster ellipticals at $z \simeq 0.4$. This sample consists of all the early-type galaxies from Ziegler et al. (1999), drawn from five clusters observed with WFPC2 — Abell 370 ($z = 0.375$), Cl 1447+26 ($z = 0.389$), Cl 0939+47 ($z = 0.407$), Cl 0303+17 ($z = 0.416$) and Cl 0016+16 ($z = 0.55$). Ziegler et al. (1999) corrected their data to zero-redshift B -band, and compared the differences in average surface brightness (ΔM) between the $z \simeq 0.4$ clusters and the Coma cluster (they used two different samples of Coma data and two different measures of average surface brightness). Ziegler et al. (1999) demonstrated that the slope of the Kormendy relation for each of these clusters was consistent with that of Coma, and that the difference in surface brightnesses ΔM was due to passive evolution of the stellar populations, possibly with some low-level ongoing star formation. In Fig. 7 we plot their fully corrected data for our cosmology, using the ‘ComaSBD/ ΔM_{free} ’ surface brightness corrections from their table 4 (taking their alternative ΔM values does not change our results). Using a least-squares bisector fit (Isobe et al. 1990) we find the best-fitting Kormendy relation for the combined sample to be $\langle \mu_e \rangle = (2.8 \pm 0.2) \log r_e + (19.4 \pm 0.1)$.

For each of the two LBDS radio galaxies, we have measured the mean surface brightness within r_e from the F110W data (Table 2) and corrected these $\langle \mu_e \rangle$ values to zero redshift. Specifically, we applied corrections of: (i) +1.8 mag K-correction from observed F110W to restframe B ; (ii) +1.5 mag of passive evolution from 3 Gyr ($z = 1.5$) to 13 Gyr ($z = 0$); (iii) -0.7 mag AB to Vega systems; and (iv) -4.0 mag due to cosmological surface brightness dimming. The combined error in these corrections is ± 0.3 mag, noting that most of the uncertainty in the models occurs at early ages and thus the error is no larger than that in the previous section. 53W069 (solid square) and 53W091 (solid circle) are overplotted on the cluster Kormendy relation in Fig. 7. The LBDS galaxies lie on the Kormendy relation, entirely consistent with the scatter in the relation for cluster ellipticals.

Our investigations of the Kormendy relation indicate that 53W069 & 53W091 are passively-evolving, dynamically-relaxed ellipticals at $z \simeq 1.5$. However, the results of Ziegler et al. (1999) show that early-type galaxies with weak disk components and low-level star formation, do not differ significantly from ellipticals on the Kormendy relation. Therefore the results of this section alone do not exclude the possibility of some star formation in the LBDS galaxies; indeed the disk component identified in 53W091 (section 3) may be the site of recent low-level star formation activity.

5 SCALING RELATIONS AND MASSES

We have shown above that the two $z \simeq 1.5$ LBDS radio galaxies 53W069 & 53W091 are significantly smaller than the average 3CR galaxy at $z \simeq 0.8$ (section 4.1). In this section, we consider whether their smaller size could also explain their lower radio luminosity. We recall how both size and radio power scale with the mass of the galaxy and its

central black hole, and then estimate of the masses of these two radio galaxies.

The correlation between the central black hole mass (M_{bh}) and the spheroid mass (M_{sph}) of galaxies is now well-established (Magorrian et al. 1998):

$$M_{\text{bh}} \propto M_{\text{sph}} \quad (1)$$

For spirals, M_{sph} is the mass of the bulge (spheroid) component (i.e. excluding the disk), for ellipticals it is the total (virial) mass of the galaxy. Further investigations have also revealed correlations between M_{bh} and spheroid luminosity (L) and between M_{bh} and stellar velocity dispersion (Kormendy & Gebhardt 2001). In the absence of velocity dispersion data we adopt the well-known relation between galaxy mass and luminosity, using the mass-to-light ratio for elliptical galaxies from Jorgensen, Franx & Kjaergaard (1996):

$$M_{\text{sph}} \propto L^{1.3} \quad (2)$$

For a de Vaucouleurs $r^{1/4}$ law, the integrated galaxy luminosity is given by $L \propto I_e r_e^2$ where the intensity at the effective radius (I_e) is trivially related to the effective surface brightness $\mu_e \propto -2.5 \log I_e$. We adopt a Kormendy relation with a slope of 3, $\mu_e \propto 3 \log r_e$, this being consistent with the 3CR results of McLure & Dunlop (2000), the cluster relation found in section 4.2 above and the $z \simeq 0.2$ AGN sample of Dunlop et al. (2002). Combining these equations thus gives a scaling relation between the effective radius and the spheroid mass of elliptical galaxies:

$$r_e \propto M_{\text{sph}}^{1.0} \quad (3)$$

The error in the index is due to errors in the $M_{\text{sph}}-L$ correlation (e.g. Kormendy & Gebhardt 2001 find $M_{\text{bh}} \propto L^{1.1}$, c.f. equations 1 & 2) and the slope of the Kormendy relation (± 0.2 , see values in section 4). The combination of these errors leads to an error in the power-law index of no more than ± 0.2 .

Whatever the physical mechanism that drives the radio output of AGN, and indeed non-active spheroids, a number of authors have found a power-law dependence between radio power (P) and black hole mass:

$$P \propto M_{\text{bh}}^\gamma \propto M_{\text{sph}}^\gamma \quad (4)$$

where we have used the Magorrian relation (equation 1) in the second step. Franceschini, Vercellone & Fabian (1998) find a best-fitting value of $\gamma = 2.7 \pm 0.3$ for a sample of nearby galaxies, whose black hole masses are based directly on stellar dynamics. They note that $\gamma \simeq 2$ is a generic prediction of any emission process that depends on the emitting area around a black hole, and in particular $\gamma = 2.2$ is the prediction of advection-dominated accretion flows (see e.g., Narayan & Yi 1995). Lacy et al. (2001) quote a value of $\gamma = 1.4 \pm 0.2$ for a sample of radio-loud quasars, although inspection of their Fig. 2 suggests $\gamma \simeq 2-2.5$ is also consistent with their data. Dunlop et al. (2002) demonstrated that with $\gamma = 2.5$, equation 4 is consistent with both (i) normal galaxies and radio-quiet quasars, and (ii) radio galaxies and radio-loud quasars, but with a normalization that differs between the two classes of radio power.

If equations 3 & 4 are combined, we get a scaling relation between the radio power and effective radius of radio-loud ellipticals:

$$P \propto r_e^{2.7} \quad (5)$$

where we have used $\gamma = 2.7$ from Franceschini et al. (1998). Given the uncertainties in γ this can only be considered an approximate relation, but it is still interesting to compare the two LBDS galaxies with the more powerful 3CR sources at $z \simeq 0.8$. We converted the observed 8.4 GHz flux densities of the ten 3CR sources (Best, Longair & Röttgering 1997) to emitted 1.4 GHz luminosities using a mean spectral index of $\alpha = 0.8$ (where $S_\nu \propto \nu^{-\alpha}$). Their mean power is then $P_{3CR} = 9 \times 10^{27} \text{ W Hz}^{-1}$ in our cosmology. We similarly calculated the 1.4 GHz luminosities of 53W069 & 53W091 (with spectral indices of 0.9 & 1.1 respectively; Waddington et al. 2000; Spinrad et al. 1997), giving $P_{LBDS} \simeq 5 \times 10^{26} \text{ W Hz}^{-1}$. Given these radio powers, and recalling that the mean effective radius of the 3CR sources is 12 kpc (section 4.1), the scaling relation (equation 4) would predict the sizes of the LBDS galaxies to be 4 kpc. This is in excellent agreement with their actual effective radii of 3 kpc. The smaller size and lower radio luminosity of these galaxies compared with 3CR is consistent with them being less-massive galaxies with proportionately less-massive black holes; their smaller size cannot be taken as evidence of evolution in the size of the largest ellipticals.

We estimated the virial masses of 53W069 & 53W091 as follows. Although we do not know the velocity dispersions, we can estimate them from the zero-redshift Fundamental Plane relation (Jorgensen et al. 1996). Using the effective radius and present-day B -band surface brightness of each galaxy derived in section 4 ($\langle \mu \rangle_e = 20.4$ for 53W069 & 20.0 for 53W091), we predict a velocity dispersion of $\sigma \simeq 150 \pm 45 \text{ km s}^{-1}$ for the LBDS galaxies. The present-day absolute B -band magnitudes (Vega system) were similarly calculated from the observed F110W magnitudes and the corrections of section 4. We find $M_B = -20.2$ for 53W069 and -20.3 for 53W091, corresponding to luminosities of $L_B = 0.9L_B^*$ and $1.0L_B^*$ respectively (Madgwick et al. 2002). Using the Faber-Jackson relation recently measured for Coma and three $z \simeq 0.4$ clusters (Ziegler & Bender 1997), we estimate a velocity dispersion of $\sigma \sim 180 \text{ km s}^{-1}$ for the LBDS galaxies, consistent with the more accurate determination from the zero-redshift Fundamental Plane. The virial mass, $M_{\text{vir}} \sim 5\sigma^2 r_e / G$, is inferred to be $M_{\text{vir}} \sim (0.4\text{--}1.2) \times 10^{11} M_\odot$ for each of the two galaxies. From equation (1), the mass of their central black holes is inferred to be $(1\text{--}3) \times 10^8 M_\odot$, taking the constant of proportionality to be 0.0025 (McLure & Dunlop 2001; Dunlop et al. 2002).

6 CONCLUSIONS

We have used *HST* observations of the two millijansky radio galaxies LBDS 53W069 and 53W091 to investigate their optical morphologies at $z \simeq 1.5$. In both F814W (restframe U -band) and F110W (restframe B -band) 53W069 is best described by an elliptical (de Vaucouleurs) model, of effective radius $0'.3$ or 3 kpc. The $U - B$ colour gradient indicates that the galaxy formed in a rapid burst of star formation at high redshift ($z > 5$) and has a high metallicity ($3Z_\odot$) stellar population. In F110W, 53W091 is similarly modelled as an elliptical galaxy of effective radius $0'.3$ (3 kpc). At shorter wavelengths (F814W), 53W091 is more extended, consistent with there being a faint blue disk contributing $\sim 20\%$ of the

flux within r_e . The $U - B$ colour of the galaxy within a radius of $0'.4$ indicates a high metallicity ($3Z_\odot$), high-redshift ($z > 5$) burst of star formation, whereas the metallicity falls to solar at larger radii.

Assuming passive evolution of their stellar populations, these two elliptical galaxies lie on the B -band Kormendy surface brightness–effective radius relations of both 3CR radio galaxies and cluster ellipticals. Their sizes and radio luminosities are consistent with scaling relations applied to the 3CR radio galaxies, in which both radio power and effective radius scale with galaxy mass.

Our analyses of the restframe UV spectra of these two galaxies demonstrated that they were passively-evolving ellipticals, with ages $\gtrsim 3$ Gyr at $z \simeq 1.5$ (Dunlop et al. 1996; Spinrad et al. 1997; Dunlop 1999b; Nolan et al. 2002). The age of the universe at this redshift is 4.5 Gyr in the flat, lambda-dominated cosmology that we assume here, requiring a formation redshift of $z_f \gtrsim 5$. In Peacock et al. (1998) we compared the primordial density fluctuation spectrum required by the existence of these galaxies with that inferred from Lyman- α absorbers and Lyman-break galaxies. Those results indicated a similarly high redshift of gravitational collapse, $z_c \simeq 6\text{--}8$.

Here we have demonstrated that the morphologies and internal colours of these galaxies similarly show them to be ellipticals whose last major episode of star formation was at very high redshift. These results imply that the last major merger was also some while in the past, since such an event would produce significant star formation and an irregular morphology, for which we see no strong evidence at the epoch at which we see them. Although it may be that the faint blue disk component in 53W091 is the remains of the galaxy's last merger. In this context, we note that 53W091 has several companions with similar colours, one of which has been spectroscopically confirmed to have the same redshift of 1.55 (Spinrad et al. 1997; Bunker et al. 2002). It is possible, even likely, that one or more of these companions will merge with 53W091 in the future. In contrast, 53W069 has no such companions.

We began the paper by asking how ellipticals formed – via monolithic collapse or hierarchical mergers? We end by concluding that we cannot be certain, even in the particular case of these two LBDS radio galaxies. The most likely interpretation of the data is that they have not evolved significantly since high redshifts ($z \sim 5$), save for passive stellar evolution. However, their formation could still have been via mergers at early times, and at least in the case of 53W091, it seems probably that further mergers lie ahead. What is clear, is that these radio galaxies are quite ordinary ellipticals, and if they continue to evolve passively until the present day they will become typical L^* elliptical galaxies.

ACKNOWLEDGMENTS

This work was based on observations with the NASA/ESA *Hubble Space Telescope* obtained at the Space Telescope Science Institute, which is operated by the Association of Universities for Research in Astronomy, Inc., under NASA contract NAS5-26555. Support was provided by NASA grant GO-7280.*.96A from STScI under NASA contract NAS5-26555. IW acknowledges the support of the Leverhulme

Trust. JSD acknowledges the enhanced research time afforded by the award of a PPARC Senior Fellowship. RJM acknowledges the award of a PPARC Postdoctoral Fellowship. The work of DS was carried out at the Jet Propulsion Laboratory, California Institute of Technology, under a contract with NASA.

REFERENCES

- Barger A. J., Aragón-Salamanca A., Smail I., Ellis R. S., Couch W. J., Dressler A., Oemler A., Poggianti B. M., Sharples R. M., 1998, *ApJ*, 501, 522
- Bertin E., Arnouts S., 1996, *A&A*, Suppl. Ser., 117, 393
- Best P. N., Longair M. S., Röttgering H. J. A., 1997, *MNRAS*, 292, 758
- Best P. N., Longair M. S., Röttgering H. J. A., 1998, *MNRAS*, 295, 549
- Bruzual G., Charlot S., 1993, *ApJ*, 405, 538
- Bruzual G., Magris C., 1999, in Sato K., ed., *Proc. IAU Symp. 183, Cosmological Parameters and the Evolution of the Universe*. Kluwer, Dordrecht, p. 152
- Bunker A., et al., 2002, *ApJ*, submitted
- Dey A., 1997, in Tanvir N., Aragón-Salamanca A., Wall J. V., eds, *The Hubble Space Telescope and the High Redshift Universe*. World Scientific, Singapore, p. 373
- Dickinson M., 1999, *NICMOS Data Handbook, Version 4.0*. Space Telescope Science Institute, Baltimore
- Djorgovski S., Davis M., 1987, *ApJ*, 313, 59
- Dressler A., Lynden-Bell D., Burstein D., Davies R. L., Faber S. M., Terlevich R. J., Wegner G., 1987, *ApJ*, 313, 42
- Dunlop J. S., 1999a, in Röttgering H. J. A., Best P. N., Lehnert M. D., eds, *The Most Distant Radio Galaxies*. Koninklijke Nederlandse Akademie van Wetenschappen, Amsterdam, p. 71
- Dunlop J. S., 1999b, in Bunker A. J., van Breugel W. J. M., eds, *ASP Conf. Ser. Vol. 193, The Hy-Redshift Universe: Galaxy Formation and Evolution at High Redshift*. Astron. Soc. Pac., San Francisco, p. 133
- Dunlop J. S., Peacock J. A., 1990, *MNRAS*, 247, 19
- Dunlop J. S., Peacock J. A., Spinrad H., Dey A., Jimenez R., Stern D., Windhorst R. A., 1996, *Nature*, 381, 581
- Dunlop J. S., McLure R. J., Kukula M. J., Baum S. A., O’Dea C. P., Hughes D. H., 2002, *MNRAS*, in press, (astro-ph/0108397)
- Eales S., Rawlings S., Law-Green D., Cotter G., Lacy M., 1997, *MNRAS*, 291, 593
- Eggen O. J., Lynden-Bell D., Sandage A. R., 1962, *ApJ*, 136, 748
- Ellis R. S., Smail I., Dressler A., Couch W. J., Oemler A., Butcher H., Sharples R. M., 1997, *ApJ*, 483, 582
- Fioc M., Rocca-Volmerange B., 1997, *A&A*, 326, 950
- Franceschini A., Vercellone S., Fabian A. C., 1998, *MNRAS*, 297, 817
- Franx M., Illingworth G., Heckman T., 1989, *AJ*, 98, 538
- Fruchter A. S., Hook R. N., Busko I. C., Mutchler M., 1997, in Casertano S., Jedrzejewski R., Keyes C. D., Stevens M., eds, *The 1997 HST Calibration Workshop*. Space Telescope Science Institute, Baltimore, p. 518
- Hook R. N., Fruchter A. S., 1997, in Hunt G., Payne H. E., eds, *ASP Conf. Ser. Vol. 125, Astronomical Data Analysis Software and Systems VI*. Astron. Soc. Pac., San Francisco, 147
- Isobe T., Feigelson E. D., Akritas M. G., Babu G. J., 1990, *ApJ*, 364, 104
- Jorgensen I., Franx M., Kjaergaard P., 1996, *MNRAS*, 280, 167
- Hinkley S., Im M., 2001, *ApJL*, 560, L41
- Kauffmann G., Charlot S., 1998, *MNRAS*, 294, 705
- Kormendy J., 1977, *ApJ*, 217, 406
- Kormendy J., Gebhardt K., 2001, in Wheeler J. C., Martel H., eds, *AIP Conf. Proc. Vol. 586, Relativistic Astrophysics: 20th Texas Symposium*. American Institute of Physics, p. 363
- Krist J., Hook R., 1999, *The Tiny Tim User’s Guide, Version 5.0*. Space Telescope Science Institute, Baltimore
- Kron R. G., Koo D. C., Windhorst R. A., 1985, *A&A*, 146, 38
- Lacy M., Laurent-Muehleisen S. A., Ridgway S. E., Becker R. H., White R. L., 2001, *ApJL*, 551, L17
- Lilly S. J., Longair M. S., 1984, *MNRAS*, 211, 833
- Lilly S. J., Longair M. S., Allington-Smith J. R., 1985, *MNRAS*, 215, 37
- Madgwick D. S., et al., 2002, *MNRAS*, 333, 133
- Magorrian J., et al., 1998, *AJ*, 115, 2285
- McLure R. J., Dunlop J. S., 2000, *MNRAS*, 317, 249
- McLure R. J., Dunlop J. S., 2001, *MNRAS*, 327, 199
- Menanteau F., Abraham R. G., Ellis R. S., 2001a, *MNRAS*, 322, 1
- Menanteau F., Jimenez R., Matteucci F., 2001b, *ApJ*, 562, L23
- Narayan R., Yi I., *ApJ*, 444, 231
- Nolan L. A., Dunlop J. S., Kukula M. J., Hughes D. H., Boroson T., Jimenez R., 2001a, *MNRAS*, 323, 308
- Nolan L. A., Dunlop J. S., Jimenez R., 2001b, *MNRAS*, 323, 385
- Nolan L. A., Dunlop J. S., Jimenez R., Heavens A. F., 2002, *MNRAS*, in press
- Pascarella S. M., Windhorst R. A., Keel W. C., Odewahn S. C., 1996, *Nature*, 383, 45
- Peacock J. A., Jimenez R., Dunlop J. S., Waddington I., Spinrad H., Stern D., Windhorst R. A., 1998, *MNRAS*, 296, 1089
- Peletier R. F., Davies R.L., Illingworth G.D., Davis L.E., Cawson M., 1990, *AJ*, 100, 1091
- Roche N., Eales S., Rawlings S., 1998, *MNRAS*, 297, 405
- Saglia R. P., Maraston C., Greggio L., Bender R., Ziegler B., 2000, *A&A*, 360, 911
- Schade D., Carlberg R. G., Yee H. K. C., López-Cruz O., 1996, *ApJL*, 464, L63
- Spinrad H., Dey A., Stern D., Dunlop J. S., Peacock J. A., Jimenez R., Windhorst R. A., 1997, *ApJ*, 484, 581
- Stockton A., Kellogg M., Ridgway S. E., 1995, *ApJL*, 443, L69
- Tamura N., Kobayashi C., Arimoto N., Kodama T., Ohta K., 2000, *AJ*, 119, 2134
- Taylor G. L., Dunlop J. S., Hughes D. H., Robson E. I., 1996, *MNRAS*, 283, 930
- Treu T., Stiavelli M., 1999, *ApJL*, 524, L27
- Voit M., 1997, *HST Data Handbook, Volume 1: Current Instruments, Version 3*. Space Telescope Science Institute, Baltimore
- Waddington I., Windhorst R. A., Dunlop J. S., Koo D. C.,

- Peacock J. A., 2000, MNRAS, 317, 801
- Windhorst R. A., van Heerde G. M., Katgert P., 1984, A&A, Suppl. Ser., 58, 1
- Windhorst R. A., Gordon J. M., Pascarelle S. M., Schmidtke P. C., Keel W. C., Burkey J. M., Dunlop J. S., 1994, ApJ435, 577
- Windhorst R. A., Keel W. C., Pascarelle S. M., 1998, ApJ, 494, L27
- Yi S., Brown T. M., Heap S., Hubeny I., Landsman W., Lanz T., Sweigart A., 2000, ApJ, 533, 670
- Ziegler B. L., Bender R., 1997, MNRAS, 291, 527
- Ziegler B. L., Saglia R. P., Bender R., Belloni P., Greggio L., Seitz S., 1999, A&A, 346, 13
- Zepf S. E., 1997, Nature, 390, 377
- Zirm A., et al., 1999, in Bunker A. J., van Breugel W. J. M., eds, ASP Conf. Ser. Vol. 193, The Hy-Redshift Universe: Galaxy Formation and Evolution at High Redshift. Astron. Soc. Pac., San Francisco, p. 114

This paper has been typeset from a \TeX / \LaTeX file prepared by the author.